Article

From 1D Chain to 3D Network: Tuning Hybrid II-VI Nanostructures and Their Optical Properties

Xiaoying Huang, Jing Li, Yong Zhang, and Angelo Mascarenhas

J. Am. Chem. Soc., **2003**, 125 (23), 7049-7055• DOI: 10.1021/ja0343611 • Publication Date (Web): 14 May 2003

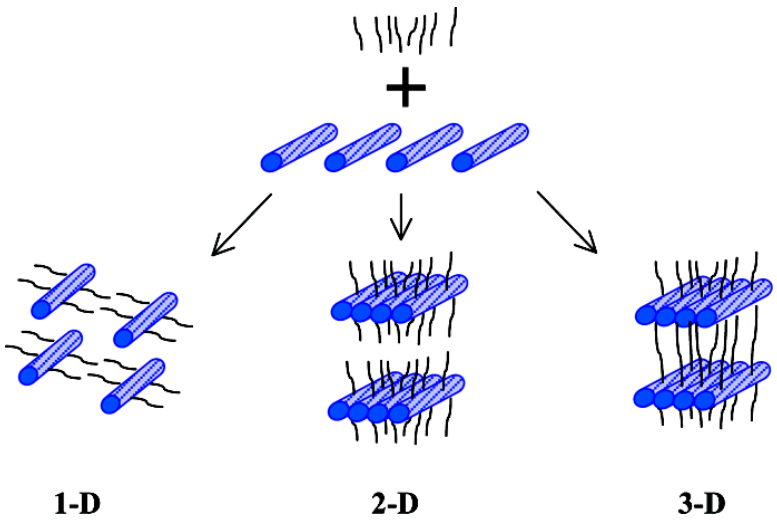

More About This Article

Additional resources and features associated with this article are available within the HTML version:

- Supporting Information
- Links to the 15 articles that cite this article, as of the time of this article download
- Access to high resolution figures
- Links to articles and content related to this article
- Copyright permission to reproduce figures and/or text from this article

View the Full Text HTML

J|A|C|S
ARTICLES
Published on Web 05/14/2003

From 1D Chain to 3D Network: Tuning Hybrid II-VI Nanostructures and Their Optical Properties

Xiaoying Huang,[†] Jing Li,*[,†] Yong Zhang,[‡] and Angelo Mascarenhas[‡]

Contrbution from the Department of Chemistry and Chemical Biology, Rutgers University, Piscataway, New Jersey 08854, and National Renewable Energy Laboratory, Golden, Colorado 80401

Received January 27, 2003; E-mail: jingli@rutchem.rutgers.edu

Abstract: In an effort to make semiconductor nanomaterials with tunable properties, we have deliberately designed and synthesized a family of novel organic−inorganic hybrid nanocomposites based on II−VI semiconductors with structures ranging from one-dimensional (1-D) chain to two-dimensional layer (2-D) to three-dimensional (3-D) framework. All nanostructures exhibit strong quantum confinement effect (QCE), while possessing a perfectly periodic arrangement. The optical absorption experiments show that all compounds generate a very large blue shift in the absorption edge (1.0−2.0 eV) due to the strong QCE. More significantly, their band edge shift and optical properties can be tuned by changing the dimensionality of inorganic motifs as well as overall crystal structures. Raman studies reveal that not only do these structures have distinctly different vibrational signatures from those of the II−VI host semiconductors, but they also differ significantly from each other as a result of changes in dimensionality. The crystal structures of these nanocomposite materials have been characterized by single crystal and/or powder X-ray diffraction methods. [ZnTe(pda)] (**1**; pda = propanediamine) is composed of 1-D chains of [ZnTe] with pda chelating to Zn atoms. [ZnTe(N_2H_4)] (**2**; N_2H_4 = hydrazine) and [ZnTe(ma)] (**3**; ma = $MeNH_2$ = methylamine) are two-dimensional (2-D) layered structures containing [ZnTe] slabs and terminal hydrazine (**2**) or methylamine (**3**) molecules. The crystal structures of [$CdSe(en)_{0.5}$] (**4**; en = ethylenediamine) and [$CdSe(pda)_{0.5}$] (**5**) are 3-D networks containing [CdSe] slabs bridged by bidentate organic diamine molecules. Crystal data for **1**: Orthorhombic, space group *Pbcm*, $a = 9.997(2)$, $b = 6.997(1)$, $c = 10.332(2)$ Å, $Z = 4$. For **2**: Monoclinic, space group $P2_1$, $a = 4.2222(6)$, $b = 6.9057(9)$, $c = 7.3031(10)$ Å, $\beta = 98.92(8)°$, $Z = 2$. For **3**: Orthorhombic, *Pbca*, $a = 7.179(1)$, $b = 6.946(1)$, $c = 18.913(4)$ Å, $Z = 8$. For **4**: Orthorhombic, *Pbca*, $a = 7.0949(3)$, $b = 6.795(3)$, $c = 16.7212(8)$ Å, $Z = 8$. For **5**: Orthorhombic, $Cmc2_1$, $a = 20.6660(12)$, $b = 6.8900(4)$, $c = 6.7513(4)$ Å, $Z = 8$.

Introduction

Semiconductor nanomaterials have been studied extensively due to their great promises in optoelectronic, magnetic, and catalytic applications.[1] When the length-scale of semiconductors is reduced to nanometer range, their chemical and physical properties exhibit dramatically different behavior from the bulk materials. Semiconductor quantum dots (QDs) and quantum wells (QWs) have attracted much attention due to their ability in modifying electronic and optical properties on large scale. To date, numerous methods have been developed to synthesize nanoparticles with desirable particle size and controlled morphologies.[2] However, it remains a great challenge to generate single-sized and periodically ordered arrays of nanostructures, which are necessary for optical devices requiring high intensity and sharp line width.[3]

To address these specific problems, we have designed a system in which nanocomponents of identical size are arranged into a perfectly periodic crystal structure. Our initial effort has resulted in a new type of 3-D hybrid nanostructures, [$MQ(L)_{0.5}$] (M = Mn, Zn; Q = Se, Te; L = en, pda).[4] Strong quantum confinement effects (QCE) are achieved when a three-dimensional II−VI semiconductor host lattice is broken into segments (MQ slices) and reconnected by organic spacers (L) via coordinate bonds. The resultant hybrid nanostructures possess three-dimensional networks that are composed of MQ monatomic (or single atomic) layers as a source of semiconductor functionality and organic diamine molecules as links and confining agents. The crystal structure of such a monatomic MQ layer can be best described as a single "slice" or "slab" cut from a II−VI parent structure, that is, a wurtzite (e.g.

[†] Department of Chemistry and Chemical Biology, Rutgers University.
[‡] National Renewable Energy Laboratory.

(1) Henglein, A. *Chem Rev.* **1989**, *89*, 1861. Steigerwald, M. L.; Brus, L. E. *Acc. Chem. Res*. **1990**, *23*, 183. Bawendi, M. G.; Steigerwald, M. L.; Brus, L. E. *Annu. Rev. Phys. Chem.* **1990**, *41*, 477. Weller, H. *Angew. Chem., Int. Ed. Engl*. **1993**, *32*, 41. Weller, H. *Adv. Mater*. **1993**, *5*, 88. Hagfeldt, A.; Gratzel, M. *Chem. Rev*. **1995**, *95*, 49. Fendler, J. H.; Meldrum, F. C. *Adv. Mater*. **1995**, *7*, 607. Alivisatos, A. P. *J. Phys. Chem*. **1996**, *100*, 13 226.
(2) Penner, R. M. *Acc. Chem. Res*. **2000**, *33*, 78. Trindade, T.; O′Brien, P.; Picket, N. L. *Chem. Mater*. **2001**, *13*, 3843.
(3) Murray, C. B.; Kagan, C. R.; Bawendi, M. G. *Science* **1995**, *270*, 1335. Nozik, A. J.; Micic, O. I. *MRS Bull*. **1998**, *23*, 24.
(4) (a) Huang, X.-Y.; Li, J.; Fu, H. *J. Am. Chem. Soc.* **2000**, *122*, 8789. (b) Huang, X. Y.; Heulings, H. R., IV; Le, V.; Li, J. *Chem. Mater*. **2001**, *13*, 3754.

Scheme 1

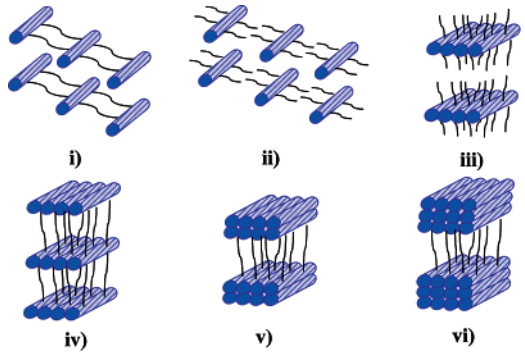

α-[ZnTe(en)$_{0.5}$]), or a zinc blende (β-[ZnTe(en)$_{0.5}$]) type, with some distortions.[4] These hybrid materials are capable of tuning electronic and optical properties of II−VI systems on the same large scale as colloidal quantum dots. Very large blue shifts in their absorption spectra are observed with respect to their II−VI parent compounds. Note that the QCE induced in these compounds is a result of inherent structure properties, thus, the restriction on size and size distribution can be lifted, and actual dimensions of the particles are not limited.

On the basis of our initial findings, we have conducted a systematic study on this new family of hybrid nanostructures. Although the length of organic spacers makes negligible effect in the optical absorption edges,[5] we anticipate significant property changes by varying the topology and dimensionality of inorganic structural motif MQ as well as overall crystal structure. Scheme 1 illustrates several possibilities, among many others: (i) MQ as 1-D chains, interconnected via organic spacers; (ii) MQ as isolated 1-D chains, coordinated to, but not interconnected by, organic groups; (iii) MQ as isolated monatomic layers; (iv) MQ as monatomic layers, interconnected; (v) MQ as bi-layers, interconnected; and (vi) MQ as trilayers, interconnected. Applying designing strategy, we have successfully prepared a number of 1-D, 2-D, and 3-D structures of these structure types. In this article, we report the synthesis and characterization of [ZnTe(pda)] (**1**; pda = propanediamine), a 1-D crystal structure containing single ZnTe chains (Type ii); [ZnTe(N_2H_4)] (**2**; N_2H_4 = hydrazine) and [ZnTe(ma)] (**3**; ma = $MeNH_2$ = Methylamine), 2-D crystal structures containing monatomic ZnTe slabs (Type iii); and [CdSe(en)$_{0.5}$] (**4**; en = ethylenediamine) and [CdSe(pda)$_{0.5}$] (**5**), 3-D crystals structures containing ZnTe monolayers (Type iv). The similarities and differences in their optical properties, the origin of such differences, and the correlation between the structures and properties, are analyzed and discussed.

Experimental Section

Materials and Instruments. $ZnCl_2$ (98%, Aldrich), $Zn(NO_3)_2{\cdot}6H_2O$ (97%, Alfa Aesar), $CdCl_2$ (99.9%, Strem), Te (99.5%, Strem), Se (99.5%, Strem), ethylenediamine (en, 99%, anhydrous, Aldrich), hydrazine (98.5%, Alfa Aesar), methylamine (40%, aqueous solution, Alfa Aesar) and 1,3-propanediamine (pda, 98%, anhydrous, Alfa Aesar). All chemicals were used as received without further purification. Powder X-ray diffraction (PXRD) of samples was performed on a Rigaku D/M-2200T automated diffraction system (Ultima$^+$). The structure analyses were carried out using SHELX97,[6] JADE (Windows), and GSAS software packages.[7] Optical diffuse reflectance spectra were measured at room temperature using a Shimadzu UV-3101PC double beam, double monochromated spectrophotometer. Raman studies were performed on a spectroscopy system with a SPEX 1403 double grating spectrometer and a cooled RCA C31034 PMT GaAs photomultiplier tube.

Synthesis of [ZnTe(pda)] (1). Single crystals of **1** were obtained by solvothermal reactions containing 0.063 g of $ZnCl_2$ (0.50 mmol) and 0.032 g of Te (0.25 mmol). The starting materials were weighed and mixed and then transferred to a thick-walled Pyrex tube. A 0.2 mL portion of 1,3-pda and 0.2 mL of hydrazine were added. After the liquid was condensed by liquid nitrogen, the tube was sealed with a torch under vacuum ($\sim 10^{-3}$ Torr). The sample was then heated at 70 °C for 10 days. After being cooled to room temperature, the mixture was washed with 30% and 80% ethanol followed by drying in anhydrous ethyl ether. Colorless platelike crystals (0.050 g, 74.9% yield based on Te) of **1** were obtained.

Synthesis of [ZnTe(N_2H_4)] (2). Reactions of $Zn(NO_3)_2{\cdot}6H_2O$ (0.149 g, 0.5 mmol), Te (0.063 g, 0.5 mmol), and hydrazine (0.3 mL) at 110 °C for 2 d in thick-wall Pyrex tubes afforded colorless columnar crystals of **2** (0.071 g, 63.0% yield based on Te). The same experimental procedure used for the synthesis of **1** was applied here.

Synthesis of [ZnTe($MeNH_2$)] (3). Compound **3** was obtained from reactions of $ZnCl_2$ (0.136 g, 1 mmol), Te (0.064 g, 0.5 mmol), and methylamine (6−9 mL) in a 23 mL acid digestion bomb at 160 °C for 7 d. The product was washed by 30% ethanol and water followed by drying in anhydrous ethyl ether. The light-gray columnar crystals of **3** (0.07846 g, 69.7% highest yield based on Te) were isolated.

Synthesis of [CdSe(en)$_{0.5}$] (4). Compound **4** was prepared from the reactions of $CdCl_2$ (0.366 g, 2 mmol), Se (0.079 g, 1 mmol), and en (6 mL) in a 23 mL acid digestion bomb at 130 °C for 8 d. The same isolation procedure for **3** was used here. The tan powder of **4** was collected in 74.5% yield (0.165 g, based on Se).

Synthesis of [CdSe(pda)$_{0.5}$] (5). Powder sample of **5** was prepared from a reaction of $CdCl_2$ (0.366 g, 2 mmol), Se (0.079 g, 1 mmol), and pda (8 mL) in a 23 mL acid digestion bomb at 130 °C for 8 d. The same isolation procedure for **3** was applied here. The tan powder of **5** (0.180 g, 78.8% based on Se) was isolated as a single phase.

Structure Analysis. Intensity data of compounds **1**, **2**, and **3** were collected at room temperature (293 ± 1 K) on an automated Enraf-Nonius CAD4 diffractometer with graphite monochromated Mo Kα radiation. Single crystals with dimensions of 0.15 × 0.06 × 0.015 mm (**1**), 0.12 × 0.02 × 0.02 mm (**2**), and 0.30 × 0.04 × 0.002 mm (**3**) were mounted on a glass fiber and placed onto the goniometer head in air. Lattice parameters were obtained from least-squares analysis of 20 computer-centered reflections with $6.11° \le \theta \le 12.83°$ (**1**), $6.81° \le \theta \le 11.35°$ (**2**), and $7.96° \le \theta \le 11.83°$ (**3**). Data collection was monitored by three standard reflections every 2 h. No decay was observed except the statistic fluctuation. Raw intensities were corrected for Lorentz and polarization effects, and for absorption by empirical method based on ψ-scan data. Direct methods yielded the position of Zn, Te atoms. Nitrogen and Carbon atoms were located from the subsequent difference Fourier maps. All non-hydrogen atoms were refined anisotropically. Hydrogen atoms were located from difference Fourier maps, and their thermal parameters were set equal to $1.2U_{eq}$ of the parent non-hydrogen atoms. The final full-matrix, least-squares refinement on F^2 converged with $R1 = 0.053$ for 709 observed reflections ($I > 2\sigma(I)$) for **1**, $R1 = 0.046$ for 1070 observed reflections ($I > 2\sigma(I)$) for **2**, and $R1 = 0.045$ for 1075 observed reflections ($I > 2\sigma(I)$) for **3**. Details of crystal parameters, data collection, and structure refinements are given in Table 1. All computations were performed

(5) Huang, X.-Y., Li, J. In *Functional Nanostructured Materials through Multiscale Assembly and Novel Patterning Techniques*; Moss, S. C., Ed.; 2002; Vol. 728, p 17−22.

(6) Sheldrick, G. M. *SHELX-97: Program For Structure Refinement*; University of Goettingen: Goettingen, Germany, 1997.

(7) Larson, A. C.; Von Dreele, R. B. *GSAS, Generalized Structure Analysis System*; Los Alamos National Laboratory: Los Alamos, New Mexico, 1998.

Table 1. Crystallographic Data for **1**, **2**, **3**

	1	**2**	**3**
empirical formula	$C_3H_{10}N_2TeZn$	H_4N_2TeZn	CH_5NTeZn
Fw	267.10	225.02	224.03
space group	Pbcm	$P2_1$	Pbca
a (Å)	9.997(2)	4.2222(6)	7.179(1)
b (Å)	6.997(1)	6.9057(9)	6.946(1)
c (Å)	10.332(2)	7.3031(10)	18.913(4)
β(°)		98.928(3)	
V (Å^3)	722.7(2)	210.36(5)	943.1(3)
Z	4	2	8
T (K)	293(2)	293(2)	293(2)
λ (Å)	0.71073	0.71073	0.71073
ρ_{calc} (g cm^{-3})	2.455	3.553	3.156
μ (mm^{-1})	7.250	12.419	11.073
$R1^a(I > 2(I))$	0.053	0.046	0.045
$R_w{}^b$	0.115	0.111	0.114

^{a} $R1 = \Sigma||F_o| - |F_c||/\Sigma|F_o|$. ^{b} $R_w = [\Sigma[w(|F_o^2| - |F_c^2|)^2]/\Sigma w(F_o^2)^2]^{1/2}$. Weighting: **1**, $w = 1/\sigma^2[F_o^2+(0.05P)^2]$, where $P = (F_o^2 + 2F_c^2)/3$; **2**, $w = 1/\sigma^2[F_o^2+(0.03P)^2+ 6.0P]$; **3**, $w = 1/\sigma^2[F_o^2+(0.075P)^2+ 0.5P]$.

Table 2. Non-Hydrogen Atomic Coordinates and Equivalent Isotropic Temperature Factors* (Å^2) for **1**, **2**, and **3**

atoms	x	y	z	U_{eq}
		1		
Zn	0.0875(1)	0.1021(2)	0.7500	0.026(1)
Te	−0.1500(1)	0.0388(1)	0.7500	0.027(1)
N	0.2064(8)	0.0330(11)	0.6093(7)	0.036(2)
C(1)	0.3518(9)	0.00002(14)	0.6254(12)	0.048(3)
C(2)	0.4040	0.0820	0.7500	0.045(4)
		2		
Zn	0.7668(3)	−0.0445(3)	0.5505(2)	0.021(1)
Te	0.7831(2)	0.3284(3)	0.6274(1)	0.019(1)
N(1)	0.831(2)	−0.164(3)	0.8168(14)	0.026(2)
N(2)	0.606(4)	−0.096(2)	0.9323(17)	0.037(3)
		3		
Zn	0.4066(1)	0.1830(1)	0.7965(1)	0.022(1)
Te	0.5646(1)	0.3091(1)	0.6796(1)	0.020(1)
N	0.5618(7)	0.3120(8)	0.8766(3)	0.028(1)
C	0.529(2)	0.255(2)	0.9485(5)	0.070(3)

*U_{eq} defined as one-third of the trace of the orthogonalized **U** tensor.

using the SHELX97 program package.[6] The final non-hydrogen atomic coordinates and the equivalent isotropic displacement parameters for **1**, **2**, and **3** are listed in Table 2.

The powder X-ray diffraction analyses of compounds **4** and **5** were performed on a Rigaku D/M-2200T automated diffraction system (Ultima$^+$). Measurements were made in a 2θ range of 8−100° for **4** and 5−100° for **5**, respectively. The data were collected at room temperature with a step size of 0.01° and a counting time of 8 s/step at the operating power of 46 kV/40 mA. The powder patterns were indexed by TREOR[8a] method using program PowderX.[8b] A careful investigation on system absences of reflections indicated the spaces groups *Pbca* for **4** and *Cmc2$_1$* for **5**, respectively. Since **4** and **5** are isostructural to $[ZnSe(en)_{0.5}]$ (**6**) and $[ZnSe(pda)_{0.5}]$ (**7**),[4] the atomic parameters of compounds **6** and **7** were input as initial values for Rietveld profile refinement in GSAS.[7] After the initial refinement of the scale, background, and unit cell parameters, the profile parameters LX, LY, trns, asym, shft, GP, stec, ptec, sfec, were refined one by one. The preferred orientation corrections were done by applying spherical harmonics function. Cd and Se atoms were refined anistropically, whereas N and C atoms were refined isotropically. Hydrogen atoms were added geometrically but were not refined. No corrections for absorption effects were made. The first (002) reflection at 10.59°(2θ) for **4** and (200) reflection at 8.646° for **5** were the strongest but highly asymmetric. This is characteristic for layered compounds. They were excluded in the final refinement. The details of the Rietveld refinements as well as crystal data are described in Table 3. Positional parameters are given in Table 4.

Table 3. Crystallographic Data for **4** and **5**

	4	**5**
empirical formula	$C_2H_8N_2Se_2Cd_2$	$C_3H_{10}N_2Se_2Cd_2$
Fw	442.82	456.85
space group	*Pbca* (No.61)	*Cmc2$_1$* (No.36)
a (Å)	7.0949(3)	20.6660(12)
b (Å)	6.795(3)	6.8900(4)
c (Å)	16.7212(8)	6.7513(4)
V (Å^3)	806.17(2)	961.31(14)
Z	4	4
T (K)	293(2)	293(2)
λ(Å)	1.5405, 1.5443	1.5405, 1.5443
ρ_{calc} (g cm^{-3})	3.648	3.157
μ (mm^{-1})	14.21	11.93
pattern range (2θ, °)	8−100	5−100
step size(2θ, °)	0.01	0.01
step scan time (s)	8	8
no. of contributing reflns. ($K\alpha_1 + K\alpha_2$)	824	568
no of struct. params.	91	94
R_{wp}	0.0643	0.0862
R_p	0.0475	0.0650
$R(F^2)$	0.0965	0.0715

Table 4. Non-Hydrogen Atomic Coordinates for **4** and **5**

atoms	x	y	z	Ueq
		compd **4**		
Cd	0.60048(16)	0.05133(17)	0.30071(7)	0.01552
Se	0.94657(23)	−0.07510(31)	0.33200(8)	0.01473
N	0.4047(17)	−0.1023(21)	0.3993(5)	0.023(4)
C	0.4051(16)	−0.0032(22)	0.4820(7)	0.031(4)
		compd **5**		
Cd	0.20998(8)	0.14845(32)	0.444(15)	0.0149
Se	0.18097(13)	0.2056(4)	0.070(15)	0.01025
N	0.1252(8)	0.3142(33)	0.598(15)	0.029(7)
C(1)	0.0614(9)	0.2476(27)	0.521(16)	0.024(8)
C(2)	0.0	0.324(4)	0.616(17)	0.026(9)

Diffuse Reflectance Measurements. Optical diffuse reflectance spectra were measured at room temperature with a Shimadzu UV-3101PC double beam, double monochromator spectrophotometer. Data were collected in the wavelength range of 250−2000 nm. $BaSO_4$ powder was used as a standard (100% reflectance). A similar procedure as previously described[9] was used to collect and convert the data using the Kubelka−Munk function.[10] The scattering coefficient (S) was treated as a constant since the average particle size of the samples used in the measurements was significantly larger than 5 μm.

Raman Experiments. A spectroscopy system with a SPEX 1403 double grating spectrometer and a cooled RCA C31034 PMT GaAs photomultiplier tube was employed in the Raman experiments. A 532 nm laser with ∼20 mW power was used as the excitation source. Spectral resolutions were typically 1−2 cm^{-1}, unless noted otherwise. Most spectra were taken at room temperature (∼300 K) with spectral resolutions of 1−2 cm^{-1}, except for one sample that was also measured at low temperature (30 K) with a resolution of 0.4 cm^{-1}.

Results and Discussion

Design and Synthesis. All compounds were synthesized via solvothermal routes. Organic amines and diamines acted as

(8) (a) Werner, P. E.; Eriksson, L.; Westdahl, M. *J. Appl. Crystallogr.* **1985**, *18*, 367. (b) Dong, C. *J. Appl. Crystallogr.* **1999**, *32*, 838.

(9) Li, J.; Chen, Z.; Wang, X.-X.; Proserpio, D. M. *J. Alloys Compd.* **1997**, *262*−*263*, 28.

(10) Wendlandt, W. M.; Hecht, H. G. *Reflectance Spectroscopy*; Interscience: A Division of John Wiley & Sons: New York, 1966.

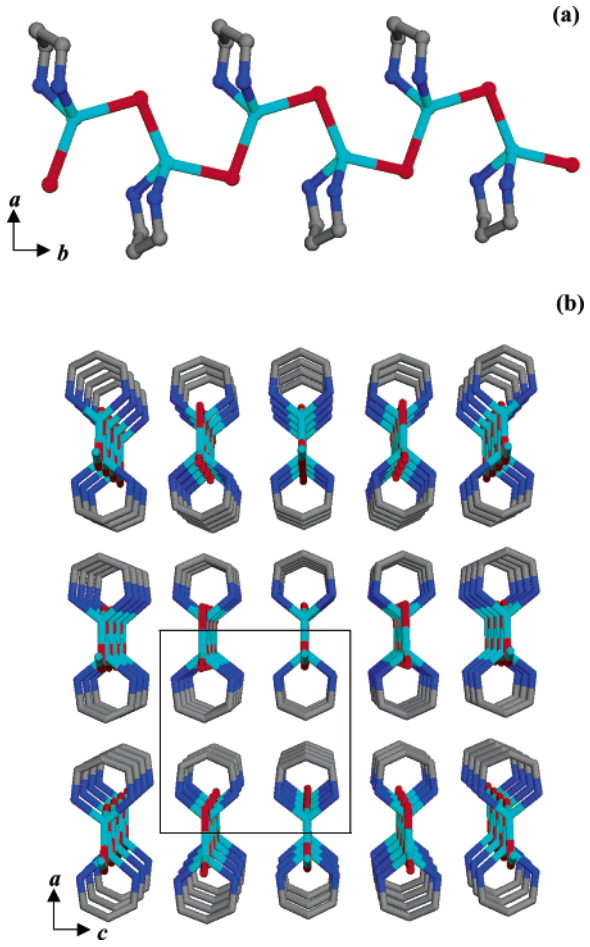

Figure 1. (a) Infinite [ZnTe(pda)] chain along *b* axis in **1**. The light-blue cylinders are Zn, red cylinders Te, blue cylinders N, and gray cylinders C, respectively. (b) View of the packing of 1D chains down *b* axis.

Scheme 2

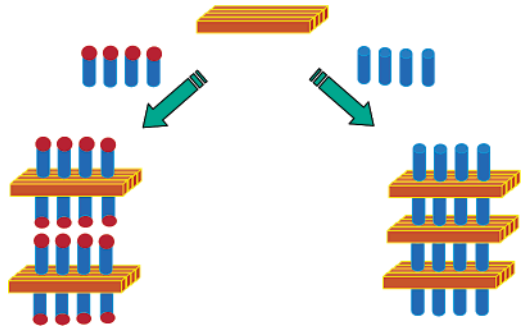

effective solvents as well as reactive reagents that entered the structures as spacers. All reactions were simple one-pot type and carried out under relatively mind conditions (70−160 °C). Single-phased samples were obtained for all compounds. The organic amines are the key components to direct the dimensionality and topology of the product compounds during the structure formation processes. Compound **1** was rationally synthesized in mixed solvents of hydrazine and pda. At higher temperatures (T > 120 °C), reactions of $ZnCl_2$ and Te with pda alone at the same ratio resulted in 3-D [ZnTe(pda)$_{0.5}$], in which the diamine molecules act as bidentate ligand bridging the two Zn metals from the adjacent ZnTe layers (Scheme 2, right). On the other hand, under the same conditions no reaction was observed at temperatures below 120 °C. Compound **1** was

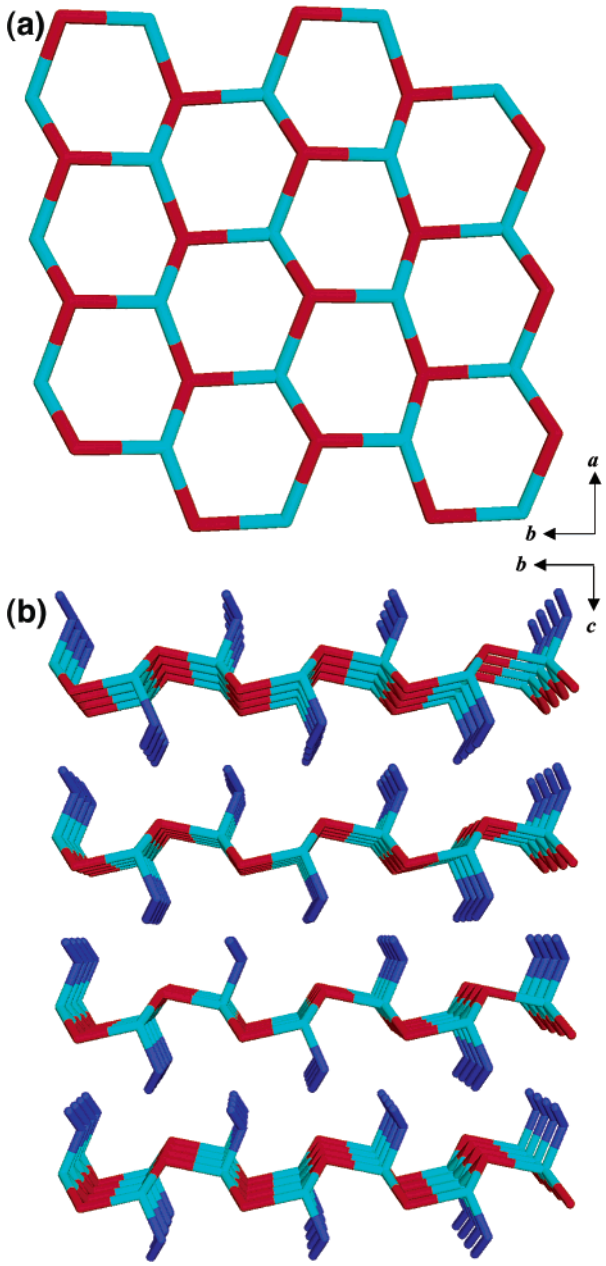

Figure 2. (a) 2-D [ZnTe] slab of **2** projected along *c* axis. The same labeling scheme as in Figure 1 is used here. (b) View of **2** along *a* axis.

obtained only by use of hydrazine as a reducing agent, which made the reactions possible at a relatively low temperature (70 °C). Under such conditions, pda molecules coordinated to metals in a chelating mode. Employing monoamine such as methylamine successfully led to 2-D layered structure **3** as shown in Scheme 2 (left). For the synthesis of compounds **4** and **5**, milder conditions were required compared to their zinc-based analogues.[4b] When the temperature was raised higher than 160 °C, binary CdSe became the major product.

Structure Description. The crystal structure of **1** is an orthorhombic system, space group *Pbcm*. It is composed of one-dimensional chains of [ZnTe(pda)] extended along *b* axis (Figure 1a). Each Zn atom is tetrahedrally coordinated to two N atoms from a chelating pda molecule and to two Te atoms. Each Te atom is bonded to two Zn atoms, thus, forming an infinite [ZnTe] chain. The angles of Zn−Te−Zn and Te−Zn−Te are

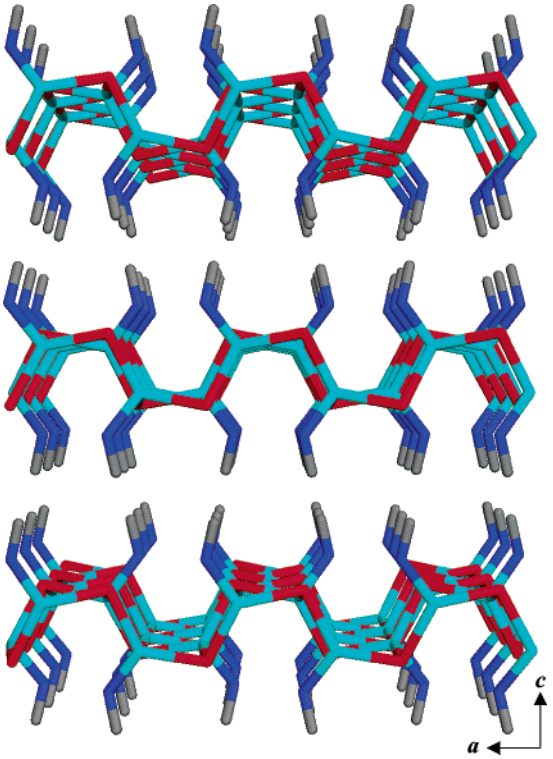

Figure 3. View of **3** along *b* axis. The same labeling scheme as in Figure 1 is used here.

98.59(4)° and 126.51(6)°, respectively. Figure 1b shows the packing fashion of [ZnTe] chains along *a*- and *c*-axis. Structure **2** belongs to monoclinic crystal system, noncentersymmetric space group $P2_1$. It is a two-dimensional network containing 2D [ZnTe] monatomic slabs and monodentate hydrazine atoms. Within the slab, Zn and Te atoms are three-coordinated to each other alternatively to form a puckered 6^3 net along *ab* plane (Figure 2a). To complete a tetrahedral configuration, each Zn atom in the slab forms its 4th bond with a nitrogen atom of hydrazine molecule. As shown in Figure 2b, the [ZnTe] slabs stack on top of each other along *c* axis with a shortest interlayer N···N distance of 3.738 Å, characteristic of VDWs interactions. Crystal structure of **3** is similar to **2**, but with hydrazine replaced by monodentate methylamine. The topology and the packing of the 6^3 nets are also slightly different from **2** (see Figures 2b and 3), which lead to an orthorhombic crystal system *Pbca*. As depicted in Figure 4, parts a and b, both compounds **4** and **5** possess a three-dimension network containing 2D single atomic [CdSe] slabs and bridging diamine molecules. The inorganic slabs are almost identical in the two structures and can be described as a single "slice" or "slab" cut from the CdSe wurtzite structure with some distortions. The only difference is in the organic pillars, with en in **4** and pda in **5**. Their room-temperature powder X-ray diffraction patterns are shown in Figure **5**, compared to the simulated patterns from GSAS refined crystal data of **4** and **5**.

Optical Diffuse Reflectance Study. The optical absorption spectra of **1**, **2** and **3** were measured by diffuse reflectance experiments,[9,10] and the results are plotted in Figure 6, along with that of zinc blende ZnTe. The absorption edges for **1**, **2** and **3** are found to be of 3.8, 3.2, and 3.5 eV, respectively. Compared to the measured value of 2.1 eV for zinc blende type ZnTe (see Table 5), it clearly indicates a very large blue shift

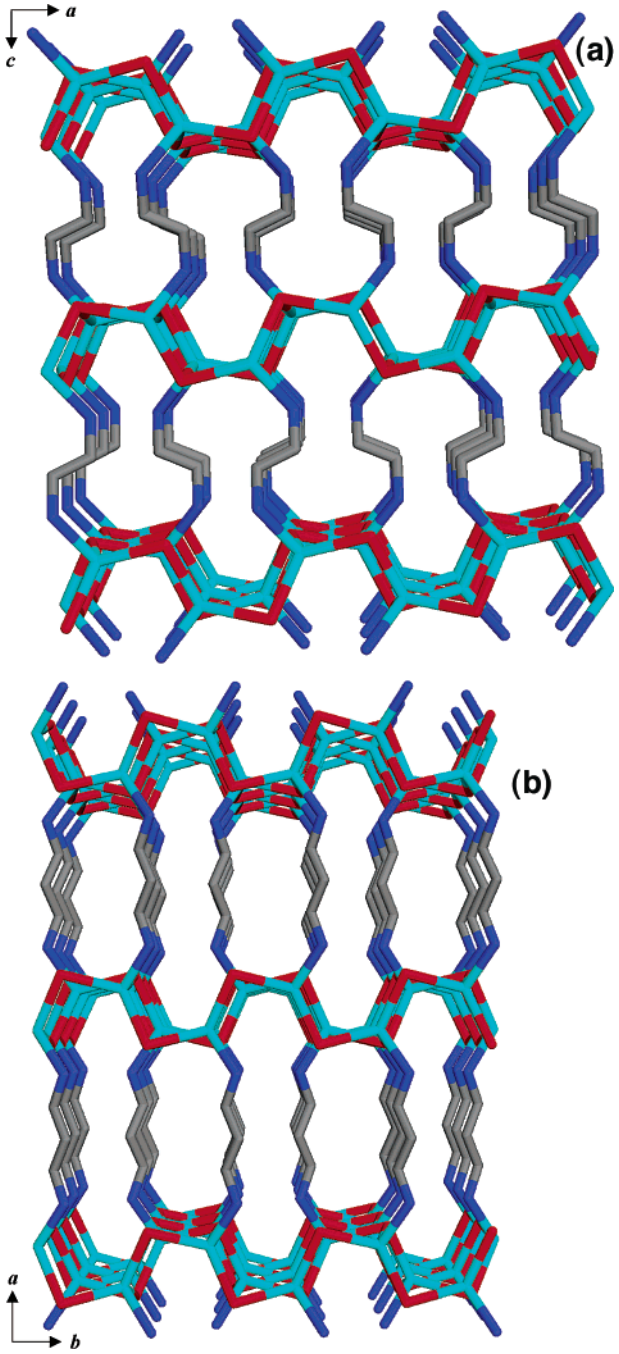

Figure 4. View of (a) **4** and (b) **5** along the *b*- and *c*-axis, respectively. The light-blue cylinders are Cd, red cylinders Se, blue cylinders N, and gray cylinders C, respectively.

(1.7, 1.1 and 1.4 eV, respectively). It is also interesting to note the extent of band edge shifts among these compounds. The absorption edges for 3-D structures α-[$ZnTe(en)_{0.5}$], *β*-[$ZnTe(en)_{0.5}$], and [$ZnTe(pda)_{0.5}$] having 2-D inorganic monolayers are 3.3, 3.5, and 3.4 eV, respectively, comparable with those of **2** and **3**, 2-D structures having a similar 2-D inorganic monolayer. Compound **1**, however, is a 1-D structure composed of 1-D inorganic component. Its band edge shift is significantly larger than any of the compounds having 2-D inorganic layers, as a result of strong confinement in two dimensions. The optical properties of **4** and **5** were also assessed by the same experiments conducted at room temperature. As shown in Figure 7, the estimated absorption edges are around 3.4−3.5 eV for both **4**

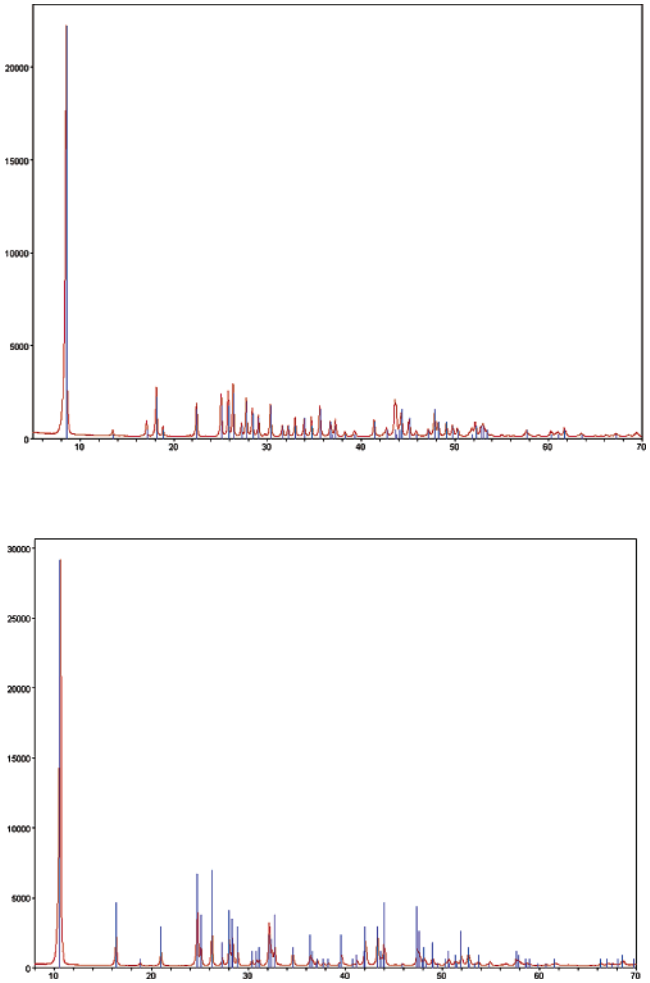

Figure 5. PXRD patterns for [CdSe(en)$_{0.5}$](top) and for [CdSe(pda)$_{0.5}$]-(bottom). The simulated powder patterns (sticks) from the GSAS Retvield refinements are shown as a comparison.

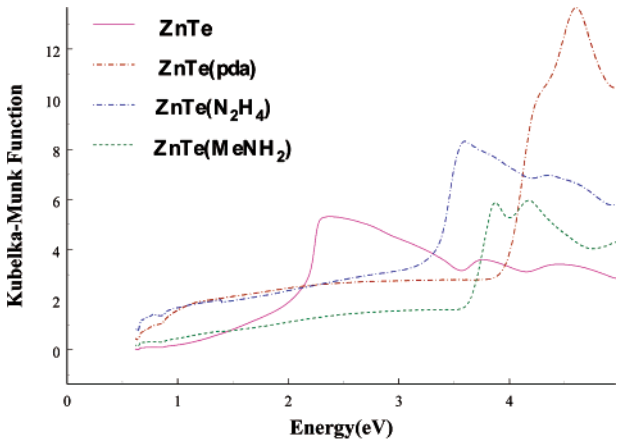

Figure 6. Optical absorption spectra for **1**(red dotted line) and **2** (blue dash−doted line), **3** (green dotted line) and bulk ZnTe (pink solid line). The estimated bang gap for ZnTe is 2.1 eV, and the onset absorption occurs at 3.8, 3.2, and 3.5 eV for **1**, **2**, and **3**, respectively.

and **5**. Compared to ∼1.6 eV measured for the CdSe bulk sample (wurzite structue) the blue shifts are as large as 1.8−1.9 eV. As a comparison, we have tabulated estimated band gap and blue-shift values of all five compounds, along with those of other II−VI hybrid compounds which we have synthesized and characterized, in Table 5. It is noteworthy that the thickness of the [ZnTe] chains in **1** and [MQ] slabs in **2**, **3**, **4**, **5** falls well below nanometer regime (5.32, 4.18, 4.99, 5.06, and 5.18 Å for **1**, **2**, **3**, **4**, **5**, respectively). Previous band structure and transition probability calculations on α-[ZnTe(en)$_{0.5}$] using density functional theory within local density approximation (LDA) have confirmed that the observed large blue shift in the optical absorption spectra is due to the quantum confinement effect (QCE) of the II−VI monolayers in the hybrid materials.[4a] Density of states (DOS) analysis has revealed these inorganic monolayers contribute dominantly to the observed band-edge absorption.

Table 5. Band Gap (BG) and Blue Shift (BS)[a] of II-VI Based Hybrid Nanostructures: 3D-[MQL$_{0.5}$] [L = Ethylenediamine(*en*); 1,3-propanediamine(*pda*); 1,4-butanediamine(*bda*); 1,5-pentanediamine(*ptda*); 1,6-hexanediamine(*hda*); Diethylenetriamine (*dien*)], 2D-[MQL] [L = Hydrazine (N_2H_4); Methylamine (*ma*); Ethylamine (*ea*); *n*-propaneamine (*n-pa*); *n*-butylamine (*n-ba*)], and 1D-[ZnTe(*pda*)]

compd	D[b]	BG (eV)	BS (eV)	compd	D[b]	BG (eV)	BS (eV)
α-[ZnS(*en*)$_{1/2}$][c]	3D	4.5	1.3	α-[CdSe(*en*)$_{1/2}$][c]	3D	3.4	1.8
ZnS(*pda*)$_{1/2}$[c]	3D	4.5	1.3	CdSe(*pda*)$_{1/2}$[c]	3D	3.5	1.9
ZnS(*bda*)$_{1/2}$[c]	3D	4.5	1.3	CdSe(*ptda*)$_{1/2}$[c]	3D	3.4	1.8
ZnS(*ptda*)$_{1/2}$[c]	3D	4.6	1.4	α-[CdTe(*en*)$_{1/2}$][c]	3D	3.1	1.7
ZnS(*hda*)$_{1/2}$[c]	3D	4.6	1.4	CdTe(*pda*)$_{1/2}$[c]	3D	3.1	1.7
ZnS(*dien*)$_{1/2}$[c]	3D	4.5	1.3	CdTe(*ptda*)$_{1/2}$[c]	3D	3.1	1.7
α-[ZnSe(*en*)$_{1/2}$][4b]	3D	4.0	1.5	α-[MnSe(*en*)$_{1/2}$][c]	3D	1.8	0.2
ZnSe(*pda*)$_{1/2}$[4b]	3D	3.9	1.4	MnSe(*pda*)$_{1/2}$[c]	3D	1.7	0.1
ZnSe(*bda*)$_{1/2}$[5]	3D	4.0	1.5	MnSe(*bda*)$_{1/2}$[c]	3D	1.8	0.2
ZnSe(*ptda*)$_{1/2}$[c]	3D	4.0	1.5				
ZnSe(*hda*)$_{1/2}$[5]	3D	4.1	1.6	ZnSe(*ma*)[c]	2D	4.0	1.5
ZnSe(*dien*)$_{1/2}$[c]	3D	4.0	1.5	ZnSe(*ea*)[c]	2D	4.0	1.5
α-[ZnTe(*en*)$_{1/2}$][4a]	3D	3.5	1.4	ZnSe(n-*pa*)[c]	2D	4.0	1.5
β-[ZnTe(*en*)$_{1/2}$][4a]	3D	3.3	1.2	ZnSe(n-*ba*)[c]	2D	4.1	1.6
ZnTe(*pda*)$_{1/2}$[4a]	3D	3.4	1.3	ZnTe(*ma*)[c]	2D	3.5	1.4
α-[CdS(*en*)$_{1/2}$][c]	3D	3.0	0.7	ZnS(N_2H_4)[c]	2D	4.3	1.2
CdS(*pda*)$_{1/2}$[c]	3D	3.0	0.7	ZnSe(N_2H_4)[c]	2D	3.7	1.2
CdS(*ptda*)$_{1/2}$[c]	3D	3.1	0.8	ZnTe(N_2H_4)[c]	2D	3.2	1.1
				ZnTe(*pda*)[c]	1D	3.8	1.7

[a] Estimated band gaps for II−VI bulk materials: CdS (wurtzite structure) 2.3 eV, CdSe (wurtzite structure) 1.5 eV, CdTe (zinc blende structure) 1.4 eV, ZnS (zinc blende structure) 3.2 eV, ZnSe (zinc blende structure) 2.5 eV, ZnTe (zinc blende structure) 2.1 eV. As an approximation, data for zinc blende structure were used when band gap values of wurtzite structure were not available. [b] D = Dimensionality. [c] This work.

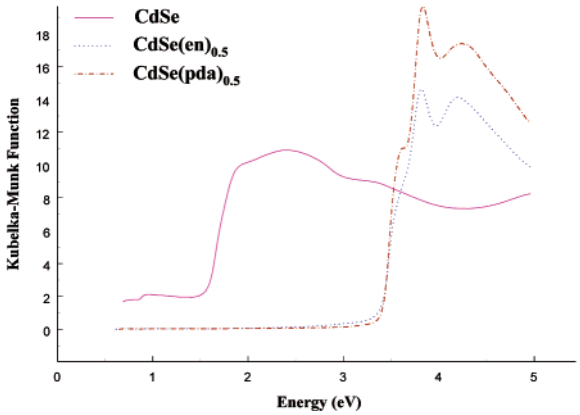

Figure 7. Optical absorption spectra for **4** (light blue line), **5** (light-red line), and bulk CdSe (pink line). The estimated bang gap for CdSe is 1.6 eV, and the onset absorption occurs at 3.4 eV, for both **4** and **5**.

Raman Study. Room-temperature Raman experiments were performed on selected crystal samples of three hybrid structures: [ZnTe(pda)] (**1**, 1-D), [ZnTe(N_2H_4)] (**2**, 2-D) and β-[ZnTe(en)$_{0.5}$] (**8**, 3-D), and compared to a reference sample of a bulk ZnTe crystal. The crystal orientations were determined

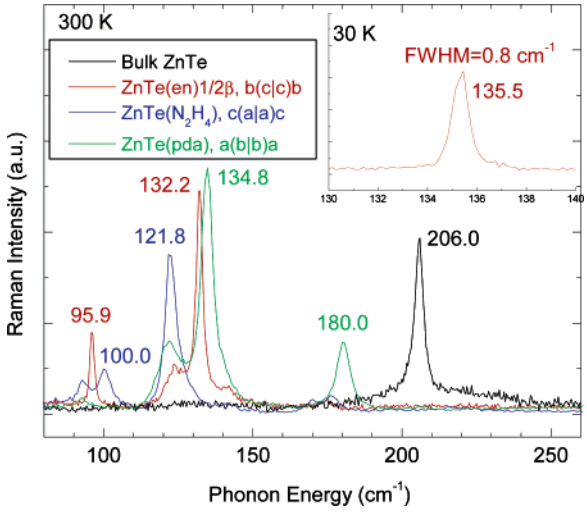

Figure 8. Raman spectra for 3-D β-[ZnTe(en)$_{1/2}$] (red), 2-D [ZnTe(N_2H_4)] (blue), and 1-D [ZnTe(pda)] (green), and bulk ZnTe (black), measured at room temperature. The insert is a low-temperature spectrum for the β-[ZnTe(en)$_{1/2}$] sample with 0.4 cm^{-1} equivalent slit width. b(c|c)b means that the excitation and detection are both along the *b* direction, and the polarization of the excitation and detection are both in the *c* direction.

by X-ray analysis. The *b*, *c*, and *a* axes were found to be perpendicular to the sample surface for **8**, **2**, and **1**, respectively. The measurements were taken in backscattering geometry. Figure 8 shows typical spectra for these crystal samples with the polarization of the excitation and detection both being in the sample plane, as indicated in the spectra. As shown in the figure, instead of the single optical phonon, LO(Γ), for the bulk sample, all three hybrid structures show multiple sharp phonon modes in frequencies very different from that of the bulk sample. They also differ significantly from each other. Qualitatively, the new features can be explained as a result of the band folding of the semiconductor related modes, similar to the situation in semiconductor superlattice,[12] as well as the coupling between the organic and inorganic species. However, detailed studies on the origin of the observed modes and their polarization dependences will be the subject of a future study. The Raman study also indicates that these hybrid structures are highly crystalline and have a high surface quality, which is evidenced by the low temperature (30 K) high-resolution data shown in the insert of Figure 8. The observed full width at half-maximum of 0.8 cm^{-1} is as small as any typical compound semiconductors at this temperature.

(11) Heulings, H. R., IV; Huang, X.-Y.; Li, J.; Yuen, T.; Lin, C. L. *Nano Lett.* **2001**, *10*, 521.
(12) Yu, P. Y.; Cardona, M. *Fundamentals of Semiconductors*; Springer: New York, 1995; Ch.9.

Summary

In this paper, we report the design, syntheses, crystal structures and optical properties of a family of hybrid II−VI semiconductor nanocomposites. Applying designing strategy, one-dimensional, two-dimensional and three-dimensional periodically ordered nanostructures with chainlike and layered inorganic MQ structural motifs are generated under mild solvothermal conditions. All compounds exhibit large blue shift in their optical absorption edges comparable to, and in most cases more so than, that of the smallest quantum dots, as illustrated by estimated band gaps and blue shifts summarized in Table 5.[4,5,11] The extent of QCE and consequently band edge shifts are determined by the dimensionality and topology of these nanostructures. Their Raman spectra show interesting features that are very different from those of II−VI bulk and vary significantly among themselves. The reported hybridization approach offers a realistic and effective alternative for tuning semiconductor electronic and optical properties, while retaining the degree of the crystalline uniformity of the binary semiconductor, as comparing to other conventional or more frequently used ways (for instance, alloying and forming semiconductor heterostructures) that usually come with significant structural fluctuations and thus the inhomogeneous broadening in spectroscopic features. This study shows that by controlling the dimensionality and topology of the II−VI inorganic component using organic spacers, hybrid nanostructures with tunable optical properties can be effectively designed and fabricated to meet the specific needs in device applications. In addition, as the QCE induced in these systems is a result of inherent crystal structure properties, the requirement on the particle size is completely lifted, giving technical advantage in the synthesis. Furthermore, incorporation of functionalities from both inorganic and organic components make them very promising as multifunctional materials in advanced technology.

Acknowledgment. Financial support from the National Science Foundation (Grant No. DMR-0094872) is gratefully acknowledged. We also thank Dr. H. -X. Fu for helpful discussions.

Supporting Information Available: Three X-ray crystallographic files (CIF). This material is available free of charge via the Internet at http://pubs.acs.org.

JA0343611